Atomic antiferromagnetic domain wall propagation beyond the relativistic limit

Huanhuan Yang,[1] H. Y. Yuan,[2,*] Ming Yan,[3] H. W. Zhang,[1] and Peng Yan[1,†]

[1]*School of Electronic Science and Engineering and State Key Laboratory of Thin Films and Integrated Devices, University of Electronic Science and Technology of China, Chengdu 610054, China*

[2]*Department of Physics, Southern University of Science and Technology, Shenzhen 518055, Guangdong, China*

[3]*Department of Physics, Shanghai University, Shanghai 200444, China*

(Received 16 December 2018; revised manuscript received 12 May 2019; published 8 July 2019)

We theoretically investigate the dynamics of atomic domain walls (DWs) in antiferromagnets driven by a spin-orbit field. For a DW with a width of a few lattice constants, we identify a Peierls-like pinning effect, with the depinning field exponentially decaying with the DW width, so that a spin-orbit field moderately larger than the threshold can drive the propagation of an atomic DW in a stepwise manner. For a broad DW, the Peierls pinning is negligibly small. However, the external spin-orbit field can induce a fast DW propagation, accompanied by a significant shrinking of its width down to atomic scales. Before stepping into the pinning region, noticeable spin waves are emitted at the tail of the DW. The spin-wave emission event not only broadens the effective width of the DW but also pushes the DW velocity over the magnonic barrier, which is generally believed to be the relativistic limit of the DW speed. While the existing dynamic theory based on the continuum approximation fails in the atomic scale, we develop an energy conversion theory to interpret the DW dynamics beyond the relativistic limit.

DOI: 10.1103/PhysRevB.100.024407

I. INTRODUCTION

Manipulating the domain wall (DW) dynamics by various knobs [1–17] is of particular importance for both fundamental interest and its useful applications in spintronic devices [18,19]. In ferromagnets, the DW velocity typically increases with the external driving force at first and then drastically decreases over a critical value, known as the Walker breakdown. Such a breakdown largely limits the maximum speed and therefore hinders the potential of applications [20]. Their antiferromagnetic counterpart, however, does not suffer from this issue. Its propagation speed can keep increasing until the magnon velocity, which is close to tens of kilometers per second [21,22]. It was shown that the DW width significantly shrinks when its velocity approaches the magnonic barrier, known as the Lorentz contraction [23–25]. The antiferromagnetic DW dynamics thus resembles the relativistic motion of a classical particle. However, the DW width should be limited by the intrinsic lattice constant due to the discrete nature of the crystal. Then it is intriguing to ask whether there is a generic cutoff of DW velocity in the antiferromagnet crystal. The static and dynamic properties of atomic DWs in ferromagnets have been well studied [26–28]. However, the antiferromagnetic DW, particularly its dynamics, in such atomic scales has received little attention from the community [29].

In this paper, we take the first step to theoretically study the dynamics of atomic antiferromagnetic DWs under a spin-orbit field. We identify a generic pinning effect in a clean system without any disorders or defects, which originates from the Peierls-like potential. The critical field for a DW propagation scales exponentially with the DW width. Under a large driven force, we find that, surprisingly, the DW could move even faster than the magnon velocity, which is in sharp contrast to the general belief of the community. Detailed analysis uncovers the critical role of strong spin-wave emissions accompanying the DW tail. In the following, our model and main results are presented in Sec. II, followed by the illustrations of damping and the thermal effect on the DW motion in Secs. III and IV, respectively. Terahertz-pulse-driven DW propagation beyond the relativistic limit is shown in Sec. V. A detailed discussion of the spin Cherenkov effect and intersublattice damping effect during DW propagation, together with the conclusions, is given in Sec. VI.

II. MODEL AND MAIN RESULTS

We consider a two-sublattice antiferromagnet with the easy axis along the longitudinal direction (z axis), as shown in Fig. 1(a). A head-to-head DW locates at the center of the system initially and then is driven to move under a Néel field ($\mathbf{H}_a = -\mathbf{H}_b = H\mathbf{e}_z$) from the spin-orbit coupling [21,30]. Figure 1(b) shows the DW velocity as a function of field strength H at various anisotropies, while the inset shows the anisotropy dependence of the DW width. Two important features can be identified: (i) When the anisotropy of the system is stronger than ∼4 meV, there exists an intrinsic pinning field. (ii) At smaller anisotropies, the DW velocity keeps increasing with field and goes beyond the magnonic barrier (indicated by the dashed line), instead of being saturated, in sharp contrast to common wisdom. This observation is qualitatively the same using the parameters for Mn_2Au (see the Appendix for

*yuanhy@sustech.edu.cn
†yan@uestc.edu.cn

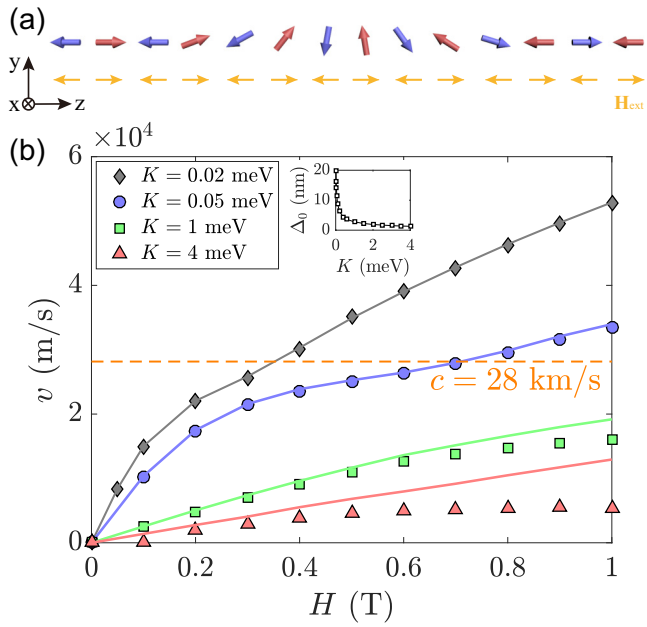

FIG. 1. (a) Schematic illustration of a two-sublattice antiferromagnet. The red and blue arrows represent the magnetic moment on each sublattice. Yellow arrows indicate the spin-orbit field. (b) The field dependence of the DW velocity for $K = 0.02$ meV (gray rhombuses), 0.05 meV (blue dots), 1 meV (green squares), and 4 meV (red triangles). The orange dashed line represents the relativistic limit. Inset: DW width as a function of the magnetic anisotropy.

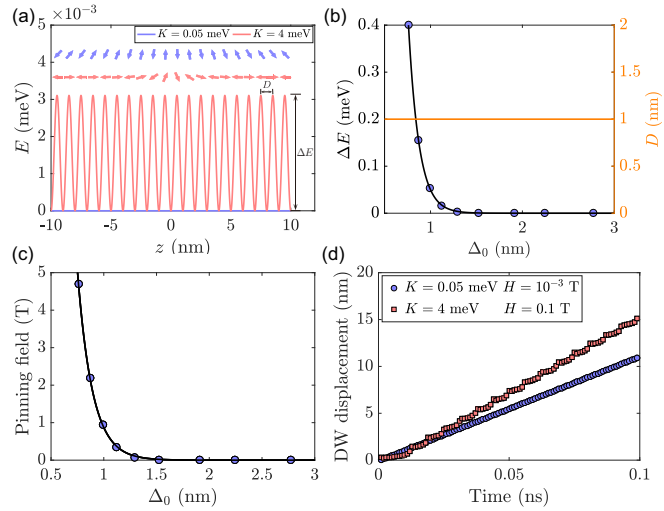

FIG. 2. (a) The Peierls-like energy profile of the DW when the DW center is placed at different positions of the nanowire for $K = 0.05$ meV (blue line) and $K = 4$ meV (red curve). Inset: The corresponding spin profile of the static domain wall. (b) The potential depth (blue dots) and period (orange line) as a function of DW width. (c) The scaling of the pinning field as a function of DW width. The black curve is the theoretical fitting. (d) The time dependence of DW displacement for $K = 0.05$ meV (blue dots) and $K = 4$ meV (red squares). The DW position is defined as the position of spin with $n_y = 1$.

detailed simulation results for Mn_2Au). Below, we examine these two features in detail.

A. Intrinsic pinning

Let us first prove that the intrinsic pinning is absent in a continuum theory by starting from the Heisenberg Hamiltonian

$$H_t = J\sum_{\langle i,j\rangle}\mathbf{S}_{ai}\cdot\mathbf{S}_{bj} - K\sum_i\left(\mathbf{S}_{ai,z}^2+\mathbf{S}_{bi,z}^2\right) - \sum_i(\mathbf{S}_{ai}\cdot\mathbf{H}_a+\mathbf{S}_{bi}\cdot\mathbf{H}_b), \quad (1)$$

where $\mathbf{S}_{ai}$ and $\mathbf{S}_{bj}$ ($|\mathbf{S}_{ai}| = |\mathbf{S}_{bj}| = S$) are the spins on sublattices a and b, respectively, and $\langle i, j\rangle$ denotes the nearest-neighboring sites. The first, second, and third terms in Eq. (1) are the exchange coupling ($J > 0$), magnetic anisotropy ($K > 0$), and Zeeman energy, respectively. In the simulations, with a fixed exchange constant $J = 16$ meV and various anisotropies and external magnetic fields, we numerically solve the Landau-Lifshitz-Gilbert (LLG) equation with homemade codes and further check the results using MUMAX3 [31].

In terms of the magnetization $\mathbf{m} \equiv (\mathbf{S}_{ai} + \mathbf{S}_{bi})/2S$ and the stagger order $\mathbf{n} \equiv (\mathbf{S}_{ai} - \mathbf{S}_{bi})/2S$, the Hamiltonian density $\mathcal{H}$ in the continuum limit [$H_t \equiv \int(dz/d)\mathcal{H}$] is given by [24,32]

$$\mathcal{H} = \frac{a}{2}\mathbf{m}^2 + \frac{A}{2}(\partial_z\mathbf{n})^2 - \frac{K_z}{2}n_z^2 + L\mathbf{m}\cdot\partial_z\mathbf{n} - 2\mathbf{n}\cdot\mathbf{H}, \quad (2)$$

where $a \equiv 8JS^2$ and $A \equiv d^2JS^2$ are, respectively, homogeneous and inhomogeneous exchange constants, with d being the lattice constant; $K_z \equiv 4KS^2$; and $L \equiv 2dJS^2$ breaks the parity symmetry and results in a net magnetic moment inside the antiferromagnetic (AFM) DW [33,34].

Minimizing the Hamiltonian with respect to the order parameters leads to the following equation:

$$\frac{A}{2}\frac{\partial^2\theta}{\partial z^2} - K_z\sin\theta\cos\theta - 2H\sin\theta = 0, \quad (3)$$

where θ is the polar angle of the stagger order in spherical coordinates. In the absence of external field, this equation naturally gives the Walker profile [1]: $\ln\tan(\theta/2) = z/\Delta_0$, with $\Delta_0 = \sqrt{A/2K_z}$ being the static DW width. With external field, we can integrate both sides of the equation and find that H should be zero to validate Eq. (3), which apparently contradicts the finite-field assumption. This implies that Eq. (3) cannot be true under finite fields; that is, a DW will always move in a clean system without any disorders or notches.

Note that the absence of pinning is purely concluded from the continuum model, which is well justified only if the length scale of the magnetic structure is much larger than the lattice constant, i.e., $\Delta_0 \gg d$. However, if the DW width is comparable to the lattice constant, the DW will need to keep adjusting its internal structure to move across the lattice and may be pinned by the lattice if the energy provided by the external driving is not sufficient. To illustrate this point, we plot the system energy as a function of DW position in Fig. 2(a), for various DW widths. Clearly, as the DW width approaches the lattice constant, the DW energy becomes strongly dependent on the DW position, which provides a generic pinning potential for the DW motion, known as the magnetic Peierls potential [26]. The static profile of DWs

should be the solution of $\delta H_t/\delta S_i = 0$, i.e.,

$$J(S_{b,i-1} + S_{b,i}) - 2KS_{ai} - H = 0,$$
$$J(S_{a,i-1} + S_{a,i}) - 2KS_{bi} + H = 0. \quad (4)$$

The inset of Fig. 2(a) shows the spin configuration obtained by numerically solving Eqs. (4), where the DW center locates between two nearest cells, i.e., where the DW is trapped at the potential well in the energy landscape. This explains why there exists an intrinsic pinning for a static DW. Figure 2(b) shows that the pinning potential scales exponentially with the DW width with a constant period D: $\Delta E = \Delta E_0 \exp[-\Delta_0/(\zeta D)]$, where $\Delta E_0 = 293$ meV and $\zeta = 0.12$ are two fitting parameters. This scaling also suggests that ζ is a universal constant that does not depend on the anisotropy. Figure 2(c) plots the DW-width dependence of the depinning field, which can also be well described by the exponential function $H_c = H_{c0} \exp[-\Delta_0/(\zeta D)]$ with coefficients $H_{c0} = 986$ T and $\zeta = 0.14$.

Naturally, it is expected that a DW should move in a stepwise manner in such a periodic potential, which is indeed the case, as shown in Fig. 2(d). Similar behavior for ferromagnetic DWs was theoretically predicted and experimentally verified [26,27,29]. For a wide DW, the stepwise propagation behavior disappears.

B. Beyond the magnonic barrier

Next, we go to the dynamics of atomically narrow DWs. The trivial case is an atomically narrow DW trapped by the Peierls potential. However, the highly nontrivial case is that a wide DW could drastically shrink its width to an atomic scale as its speed approaches the relativistic limit due to the Lorentz contraction. In what follows, we focus on the latter case.

As shown in Fig. 1(b), the DW could propagate beyond the relativistic limit (or magnonic barrier), which suggests that the intrinsic pinning from the discrete lattice does not play a significant role for dynamical DWs. To probe this propagation mode, we plot the spin configurations at different times in Fig. 3(a), with two important features: (i) The magnetic structure behaves as a soliton or rigid body that keeps its shape unchanged during the stable propagation. (ii) The magnetization profile is no longer the Walker solution, where significant spin-wave packets are emitted only at the tail of the wall. As a comparison, Fig. 3(b) shows the case without spin-wave emission when the DW velocity is well below the magnonic barrier. The DW dynamics above and below the relativistic limit is reminiscent of the spin Cherenkov effect in a ferromagnetic cylinder [36].

Before presenting our theory on the DW motion beyond the magnonic limit, we first discuss the analytics in the continuous limit, where the steady DW motion obeys the sine-Gordon equation [24],

$$\frac{1}{c^2}\frac{\partial^2\varphi}{\partial t^2} - \frac{\partial^2\varphi}{\partial z^2} + \frac{1}{\Delta_0^2}\sin\varphi = 0, \quad (5)$$

with $\varphi = 2\theta$ and $c = \gamma\sqrt{Aa/2}$ being the magnon velocity. The one-soliton solution (DW) takes the general form $\varphi = 4\arctan\exp[(z - vt)/\Delta]$, with $\Delta = \Delta_0\sqrt{1 - v^2/c^2}$. Then one can immediately see that the maximum speed

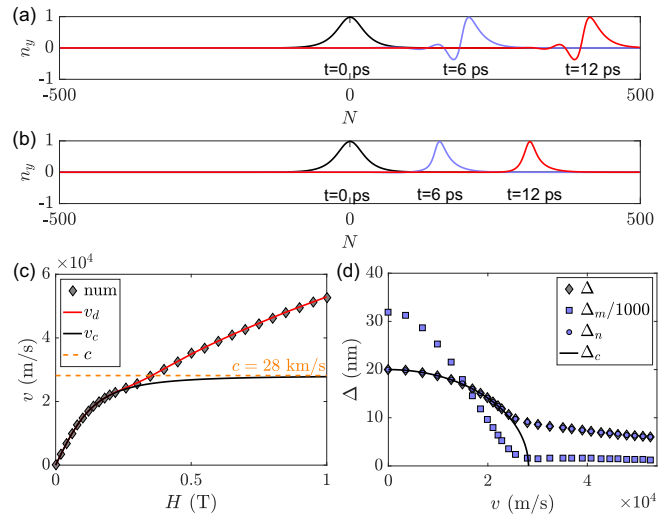

FIG. 3. (a) The profiles of magnetic structures at $t = 0$, 6, 12 ps for (a) $H = 0.5$ T and (b) 0.3 T, respectively. (c) Domain wall velocity [35] as a function of the field. Symbols are numerical results, and the red and black curves represent the prediction of a discrete model and a continuous model, respectively. The subscripts of v_d and v_c refer to the prediction of discrete and continuous models, respectively. The orange dashed line is the magnon velocity in this system. The parameters are $\Delta_0 = 20$ nm and $\alpha = 0.02$. (d) The velocity dependence of the DW width.

of the soliton is the magnon velocity when the DW width approaches zero. Our results obviously cannot be explained by the sine-Gordon theory. Tracing the numerical findings shown in Fig. 3(a), the spatial extension of the DW has reached atomic scales at high speeds, such that the spatial differential operators in Eqs. (2) and (5) are not well enough defined to replace the difference operators in Eq. (1).

These findings motivate us to abandon the continuous Hamiltonian (2) and the sine-Gordon Eq. (5) as well. The new starting point is the energy conversion and its conservation. Regardless of the detailed DW profile, the change rate of the Zeeman energy during the DW propagation should be equal to the magnetic energy dissipation rate through the Gilbert damping,

$$-2HM_s v = -\frac{\alpha d M_s}{2\gamma}\sum_i\left[\left(\frac{\partial \mathbf{S}_{ai}}{\partial t}\right)^2 + \left(\frac{\partial \mathbf{S}_{bi}}{\partial t}\right)^2\right], \quad (6)$$

where the sum is taken over all atoms. For a relatively large damping, we ignore the influence of the spin wave and discuss the damping dependence of the DW velocity in Sec. III. Since the anisotropy energy does not change for the rigid-body-like domain for the whole propagation, the anisotropy term does not enter Eq. (6). For a rigid-body motion, we have $\partial_t \mathbf{S}_{\mu i} = -\mathbf{v}\cdot\nabla_l \mathbf{S}_{\mu i}$, where $\mu = a, b$ and ∇_l is the first-order difference operator, $\nabla_l \mathbf{S}_{\mu i} = (\mathbf{S}_{\mu i} - \mathbf{S}_{\mu i-1})/d$. Then we can explicitly express the DW velocity as

$$v = \frac{\gamma H \Delta_{\text{eff}}}{\alpha}, \quad \Delta_{\text{eff}} = \frac{4}{d}\left[\sum_{\mu i}(\nabla_l \mathbf{S}_{\mu i})^2\right]^{-1}. \quad (7)$$

In the wide DW limit ($\Delta_{\text{eff}} \gg d$), we can replace the sum by the integral and the magnetic moments by the magnetization order and the stagger order, and we obtain $\Delta_{\text{eff}}^{-1} = 2\int_\Omega[(\partial_z \mathbf{m})^2 + (\partial_z \mathbf{n})^2]dz$. By disregarding the quadratic term of the magnetization and adopting the Walker approximation, we can show $\Delta_{\text{eff}} = 2/\int_\Omega (\partial_z \mathbf{n})^2 dz = \Delta$. Combining the Lorentz contraction $\Delta = \Delta_0\sqrt{1 - v^2/c^2}$ with the velocity expression $v = \gamma H \Delta/\alpha$, we obtain the DW velocity as $v = c\gamma H \Delta_0/\sqrt{\gamma^2 H^2 \Delta_0^2 + \alpha^2 c^2}$, which increases as the spin-orbit field increases but finally saturates [as plotted by the black curve in Fig. 3(c)].

When $\Delta_{\text{eff}} \sim d$, the above velocity formula is not applicable, but Eq. (7) still holds. Figure 3(c) shows that the theoretical formula (red curve) compares perfectly with numerical results over the entire spin-orbit field regime. To clarify the variation of whether the magnetization or the stagger order dominates the DW velocity in high fields, we define two DW widths, $\Delta_m = \frac{2}{d}[\sum_i (\nabla_l \mathbf{m}_i)^2]^{-1}$ and $\Delta_n = \frac{2}{d}[\sum_i (\nabla_l \mathbf{n}_i)^2]^{-1}$. Then the DW velocity can be rewritten as

$$v = \frac{\gamma H}{\alpha}\left(\frac{1}{\Delta_m} + \frac{1}{\Delta_n}\right)^{-1}. \tag{8}$$

Figure 3(d) shows that Δ_m is almost three orders of magnitude larger than Δ_n, and its contribution to the DW propagation can therefore be neglected. Moreover, Δ_n in the high-velocity regime approaches a constant value around 5 nm instead of zero as predicted by the continuum field theory. This difference comes from the spin-wave excitation at the tail of an atomic DW, which effectively broadens the DW width.

III. DAMPING EFFECT ON DOMAIN WALL MOTION

Since the magnitude of damping in antiferromagnets is still not well characterized in experiments, here we treat it as a free parameter and study its influence on the DW motion. Figure 4(a) shows the DW velocity as a function of external field for damping ranging from 0.02 to 0.0001. First, the DW velocity can go beyond the relativistic limit (orange dashed line), which indicates the robustness of our findings against the fluctuation of dampings. Second, the critical field required to exceed the magnon velocity H_c decreases and approaches 0.2 T, which is equal to the anisotropy field of the system ($H_K = 4KS^2/\mu_s = 0.4\,\text{T}$ for $K = 0.02\,\text{meV}$). This is unusual in the following way. From the DW velocity $v = \gamma H \Delta/\alpha$ obtained from the energy conversion principle, we can estimate the critical field as $H_c = \alpha c/(\gamma\Delta)$, which will keep decreasing to zero with the dampings dropping to zero, which is not consistent with Fig. 4(b). This deviation may come from the significant contribution from spin waves at low damping or nearly zero damping, as addressed in the ferromagnetic case [11]. Specifically, the inclusion of spin waves will modify the energy conservation equation as

$$-2HM_s v = -\frac{\alpha d M_s}{2\gamma}\sum_i\left[\left(\frac{\partial \mathbf{S}_{ai}}{\partial t}\right)^2 + \left(\frac{\partial \mathbf{S}_{bi}}{\partial t}\right)^2\right] - dP_{SW}, \tag{9}$$

where P_{SW} (>0) is the contribution from the emitted spin wave accompanying the DW propagation. We can solve this equation to obtain the DW velocity as

$$v = \frac{1}{2}\left[\frac{\gamma H\Delta}{\alpha} + \sqrt{\left(\frac{\gamma H\Delta}{\alpha}\right)^2 - \frac{2\gamma\Delta P_{SW}}{\alpha M_s}}\right]. \tag{10}$$

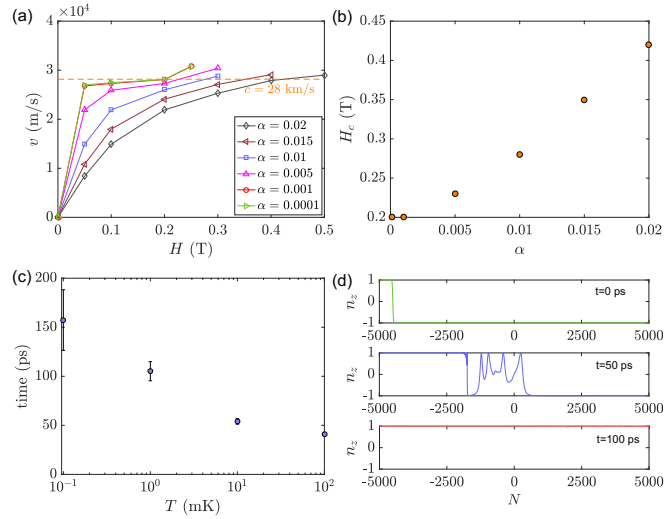

FIG. 4. (a) Domain wall velocity as a function of field for damping ranging from 0.02 to 10^{-4}. The orange dashed line is the relativistic limit. (b) Damping dependence of the critical field to exceed the magnon velocity H_c. $K = 0.02\,\text{meV}$, $T = 0\,\text{K}$. (c) Reversal time of the right domain of the nanowire as a function of temperature. $\alpha = 0.001$. (d) Snapshots of n_z vs z during a typical reversal process. $T = 1\,\text{mK}$.

With the decrease of α, the spin-wave contribution proportional to $-P_{SW}/\alpha$ becomes significant, and it will reduce the DW velocity, such that the essential field to reach the relativistic limit becomes larger. This effect will compete with the term $\gamma H/\alpha$ and results in the plateau of H_c at very low damping. Quantitative calculation of P_{SW} requires us to consider the spin-wave spectrum accompanying the DW as well as the interference of the waves. This goes beyond the scope of current work.

IV. THERMAL EFFECT ON DOMAIN WALL MOTION

To consider the influence of the thermal effect on DW dynamics, we consider the stochastic LLG equation [37],

$$\frac{\partial \mathbf{m}_i}{\partial t} = -\gamma \mathbf{m}_i \times \mathbf{h}_{i,\text{eff}} - \gamma\alpha \mathbf{m}_i \times (\mathbf{m}_i \times \mathbf{h}_{i,\text{eff}}), \tag{11}$$

where $\mathbf{m}_i$ is the magnetic vector on the ith lattice site and $\mathbf{h}_{i,\text{eff}}$ includes the exchange field, anisotropy field, spin-orbit field, and a random field ζ_i that satisfies the statistics,

$$\langle\zeta_i\rangle = 0, \quad \langle\zeta_{i,\mu}(t)\zeta_{j,\nu}(t')\rangle = \frac{2\alpha k_B T}{\gamma\mu_s}\delta(t-t')\delta_{ij}\delta_{\mu\nu}, \tag{12}$$

where Greek indices (μ, ν) refer to Cartesian coordinates x, y, z, respectively, and $\alpha, k_B, T, \mu_0, \gamma$, and μ_s are, respectively, the damping, Boltzmann constant, simulated temperature, vacuum permeability, and atomistic magnetic moment. In the simulation with a discrete time step Δt, the thermal

field is expressed as

$$\zeta_{i,\mu} = \eta\sqrt{\frac{2\alpha k_B T}{\gamma \mu_s \Delta t}}, \tag{13}$$

where η is a random number satisfying the random normal distribution with zero average. Note that $\zeta_{i,\mu} \propto \sqrt{\alpha}$; to reduce the effect of thermal field on the stability of magnetic domains, we take a smaller damping $\alpha = 0.001$.

One-dimensional case. Figure 4(c) shows the reversal time of the magnetic domain as a function of temperature, while a typical reversal process is shown in Fig. 4(d). For $T = 1$ mK, the switching time is 0.1 ns. Physically, the reversal happens because the Néel field H is opposite the stagger magnetization of the magnetic domains on the right-hand side of the DWs, and hence, it will induce the magnetic moment switching when H is comparable to the anisotropy of the system, similar to the traditional field-induced magnetization switching in a ferromagnet that can be well explained by the Stoner-Wohlfarth model [38].

Two-dimensional case. The reversal of the magnetic domain at low temperature still occurs when DW moves beyond the relativistic limit. The reason is that both the anisotropy energy and magnetic field energy are proportional to the size of the domain, and the ratio between the anisotropy field and magnetic field (H_c/H_K) determines the condition for magnetic moment switching. The extension of the system to two dimensions enlarges the domain size but does not change H_c/H_K.

In summary, the Néel-field-driven antiferromagnetic DW motion beyond the relativistic limit is a low-temperature phenomenon, and we suggest using subnanosecond current pulses with a duration shorter than the reversal time of the domains [39] to drive the DW such that the reversal can be avoided. Moreover, one can use a terahertz field-pulse (not Néel-field-like) to drive the DW propagation with better stability.

V. TERAHERTZ-FIELD-PULSE-DRIVEN DOMAIN WALL MOTION

Here we show that a terahertz field pulse can drive an antiferromagnetic DW to move beyond the relativistic limit with better thermal stability free from the magnetization reversal problem.

Figure 5(a) shows the initial 90° DW profile obtained by minimizing the sum of exchange energy and a cubic anisotropy $E_{\rm an} = K_c \sum_{i,\mu}[(S^x_\mu)^2(S^y_\mu)^2 + (S^x_\mu)^2(S^z_\mu)^2 + (S^y_\mu)^2(S^z_\mu)^2]$, $\mu = a, b$. Then a terahertz field pulse with maximum amplitude H is applied in the longitudinal direction (z axis) to drive the DW. Figure 5(b) shows that the DW velocity increases with the field amplitude H and goes beyond the relativistic limit for $H > 4$ T. Since the field is normal to the direction of the magnetic domain, the spin-flop transition does not occur. Figure 5(c) shows that the propagation mode is robust up to the temperature $T = 1$ K. The stability regime can survive up to 10 K in a two-dimensional film with the same parameters as its one-dimensional counterpart. Note that a terahertz field pulse with the desired shape can be realized [40], and our proposal should be applicable to metals, insulators, and semiconductors.

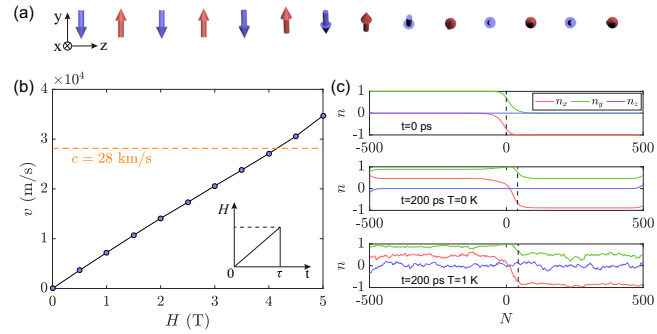

FIG. 5. (a) Schematic illustration of a two-sublattice antiferromagnet with a 90° DW that separates two domains along $n_y = 1$ and $n_x = -1$. The terahertz field pulse $H(t) = \theta(\tau - t)\theta(t)Ht/\tau$ is applied along the z direction with maximum magnitude H and duration τ, where $\theta(t)$ is a step function. (b) Domain wall velocity as a function of H. $J = 16$ meV, $K_c = 0.02$ meV, $\alpha = 0.001$. The dashed line represents the relativistic limit. The bottom inset shows the shape of the field pulse. (c) Domain wall profile as a function of time at $\tau = 2$ ps for $T = 0$ and 1 K, respectively. The vertical dashed line indicates the position of DWs. The DW displacement is the same for $T = 0$ K and $T = 1$ K, and no magnetization reversal is found when the simulation time increases further.

VI. DISCUSSION AND CONCLUSION

First, we would like to compare our results with the supermagnonic phenomena in a cylindrical ferromagnetic nanowire, where spin waves are emitted in both the front and tail of the DWs with different frequencies but share an equal phase velocity [36,41]. In our case, spin waves are emitted only at the tail of the DW. This difference can be understood from the distinct natures of ferromagnetic and antiferromagnetic spin-wave dispersions, as shown in Figs. 6(a) and 6(b). In a ferromagnet, there exist two spin-wave modes for a given phase speed (DW speed), while the group velocity of the high- (low-) frequency mode is larger (smaller) than the DW speed [as plotted in Fig. 6(c)]. Hence, the high-frequency mode runs in front of the DW, while the low-frequency one lags behind. For an antiferromagnet, only one spin-wave mode exists at a given phase speed, and its group velocity is always smaller than its phase velocity [DW speed; see Fig. 6(d)]. So it always lags behind the wall. Further, from the perspective of materials, a cylindrical geometry is required to eliminate the Walker breakdown effect and to accelerate the DW into the magnonic regime, while it is still a challenge to make a perfect cylindrical magnetic wire and to detect the nanoscale DW motions in particular. However, for antiferromagnets, a planar film is sufficient to reach this magnonic regime with a typical DW velocity as high as several tens of kilometers per second, 10 times faster than the speed in ferromagnets.

Second, the dissipation mechanism of spins is a long-lasting issue in general magnetism. The effect of intersublattice pumping on magnetic damping was first uncovered by Yuan *et al.* [43] on antiferromagnets and then was extended to ferrimagnets by Kamra *et al.* [44]. The existence of the intersublattice pumping will make the damping coefficient through the motion of magnetization sufficiently larger than that of the Néel order, which was verified by two independent

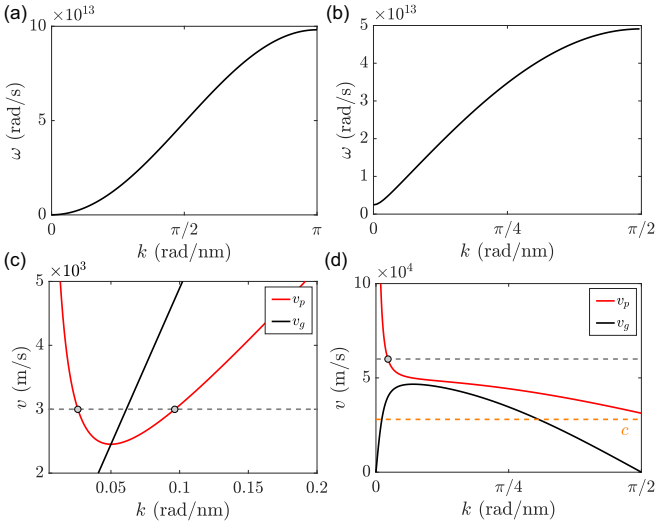

FIG. 6. Spin-wave spectrum in (a) ferromagnets and (b) antiferromagnets. The k dependence of the phase velocity (red curve) and the group velocity (black curve) for (c) ferromagnetic and (d) antiferromagnetic spin waves. The parameters $J = 16$ meV and $K = 0.02$ meV are used for both ferromagnets and antiferromagnets for a fair comparison. The gray (orange) dashed lines refers to a speed beyond (at) the relativistic limit [42].

first-principles calculations [45,46], while the experimental evidence is still lacking. Back to our concern, the intersublattice damping will influence Eq. (6) as

$$-2HM_s v = -\frac{dM_s}{2\gamma}\sum_i\left[\left(\alpha\frac{\partial \mathbf{S}_{ai}}{\partial t}\right)^2+\alpha\left(\frac{\partial \mathbf{S}_{bi}}{\partial t}\right)^2 + 2\alpha_c\left(\frac{\partial \mathbf{S}_{ai}}{\partial t}\right)\cdot\left(\frac{\partial \mathbf{S}_{bi}}{\partial t}\right)\right], \tag{14}$$

where α_c is the intersublattice damping coefficient. Similar to the procedure in Sec. II, we obtain the DW speed as

$$v = \gamma H\left(\frac{\alpha_m}{\Delta_m}+\frac{\alpha_n}{\Delta_n}\right)^{-1}, \tag{15}$$

where $\alpha_m = \alpha + \alpha_c$, $\alpha_n = \alpha - \alpha_c$, $\Delta_m = \frac{2}{d}[\sum_i (\nabla_l \mathbf{m}_i)^2]^{-1}$, and $\Delta_n = \frac{2}{d}[\sum_i (\nabla_l \mathbf{n}_i)^2]^{-1}$. Numerical simulations show that $\Delta_m \sim 10^3\Delta_n$, while the first-principles calculation gives $\alpha_m \sim 10\alpha_n$–$10^3\alpha_n$. Hence, the influence of the intersublattice damping should have a minor effect on the velocity if $\alpha_m \sim 10\alpha_n$–$10^2\alpha_n$, while it may lead to a sizable DW velocity reduction if $\alpha_m \sim 10^3\alpha_n$. This suggests to us a practical method to quantify the intersublattice damping by measuring the DW velocity in future experiments.

Third, chiral damping was shown to exist in noncentrosymmetric ferromagnetic systems [47–50], while its manifestation in an AFM and its subsequent influence on the DW velocity are still open questions.

Last, it was shown that the antiferromagnetic DW could survive in the quantum limit and the spins inside the DW become highly entangled. In our current model, spin-spin entanglement may be neglectably small since we are dealing with a classical spin system where spins are approximated as classical vectors [34]. On the other hand, the quantum effect may reduce the spin length and thus increase the effective DW width in Eq. (7), which tends to further increase DW speed. This effect may become pronounced in low-spin cases.

In conclusion, we have investigated both the static and dynamic behaviors of atomic DWs in antiferromagnets. An intrinsic pinning effect was identified due to the discrete nature of crystal lattices instead of disorders or defects. Driven by an external field larger than the pinning force, the DW velocity could go beyond the relativistic limit. Since the required spin-orbit field is comparable with the domain anisotropy, a stable supermagnonic DW propagation is observable only at very low temperatures. Nevertheless, one may use either the subnanosecond spin-orbit field pulse (duration smaller than the switching time) or the normal terahertz field pulse (not the Néel field), to enhance the DW stability against thermal fluctuations and to avoid the domain flipping [39]. This finding suggests that the antiferromagnetic domain wall motion beyond the relativistic limit should be a quite general phenomenon, which roots in the discrete nature of the lattice.

ACKNOWLEDGMENTS

H.Y.Y. is financially supported by the National Natural Science Foundation of China (NSFC) under Grant No. 61704071 and the Shenzhen Fundamental Subject Research Program under Grant No. JCYJ20180302174248595. M.Y. is supported by NSFC under Grant No. 11774218. P.Y. is partially supported by NSFC under Grant No. 11604041.

APPENDIX: SIMULATION RESULTS ON Mn_2Au

Figure 7 shows the DW velocity as a function of field strength using the parameters for Mn_2Au, i.e., $J = 24$ meV

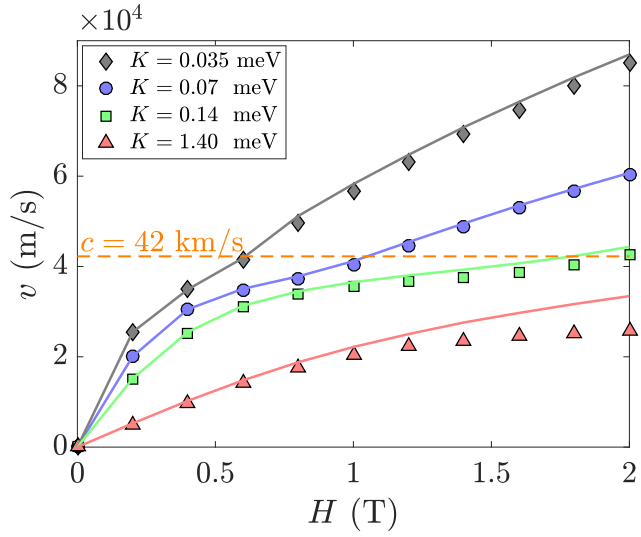

FIG. 7. Domain wall velocity as a function of field strength for $K = 0.035$ meV (gray diamonds), 0.07 meV (blue circles), 0.14 meV (green squares), and 1.40 meV (red triangles). The solid lines are theoretical predictions. The dashed line at $c = 42.24$ km/s indicates the relativistic limit.

[51] and $\mu_s = 3.59\mu_B$. Since the anisotropy of Mn_2Au is sensitive to the magnitude of strain (0.07 meV per 1% strain [52]), we take three different values of anisotropy for comparison. For larger anisotropy (larger strain), the pinning effect hinders the DW propagation. For smaller anisotropy (weak strain), the DW velocity can go beyond the relativistic limit. These results are qualitatively the same as shown in Fig. 1 of the main text. It is therefore safe to claim that our results are applicable to a wide class of antiferromagnets, including Mn_2Au.

[1] N. L. Schryer and L. R. Walker, The motion of 180° domain walls in uniform dc magnetic fields, J. Appl. Phys. **45**, 5406 (1974).

[2] X. R. Wang, P. Yan, J. Lu, and C. He, Magnetic field driven domain-wall propagation in magnetic nanowires, Ann. Phys. (N.Y.) **324**, 1815 (2009).

[3] S. Zhang and Z. Li, Roles of Nonequilibrium Conduction Electrons on the Magnetization Dynamics of Ferromagnets, Phys. Rev. Lett. **93**, 127204 (2004).

[4] G. Tatara and H. Kohno, Theory of Current-Driven Domain Wall Motion: Spin Transfer versus Momentum Transfer, Phys. Rev. Lett. **92**, 086601 (2004).

[5] A. Thiaville, Y. Nakatani, J. Miltat, and Y. Suzuki, Micromagnetic understanding of current-driven domain wall motion in patterned nanowires, Europhys. Lett. **69**, 990 (2005).

[6] M. Kläui, P.-O. Jubert, R. Allenspach, A. Bischof, J. A. C. Bland, G. Faini, U. Rüdiger, C. A. F. Vaz, L. Vila, and C. Vouille, Direct Observation of Domain-Wall Configurations Transformed by Spin Currents, Phys. Rev. Lett. **95**, 026601 (2005).

[7] A. Manchon and S. Zhang, Theory of spin torque due to spin-orbit coupling, Phys. Rev. B **79**, 094422 (2009).

[8] I. M. Miron, T. Moore, H. Szambolics, L. D. Buda-Prejbeanu, S. Auffret, B. Rodmacq, S. Pizzini, J. Vogel, M. Bonfim, A. Schuhl, and G. Gaudin, Fast current-induced domain-wall motion controlled by the Rashba effect, Nat. Mater. **10**, 419 (2011).

[9] S. Emori, U. Bauer, S.-M. Ahn, E. Martinez, and G. S. D. Beach, Current-driven dynamics of chiral ferromagnetic domain walls, Nat. Mater. **12**, 611 (2013).

[10] P. Yan, X. S. Wang, and X. R. Wang, All-Magnonic Spin-Transfer Torque and Domain Wall Propagation, Phys. Rev. Lett. **107**, 177207 (2011).

[11] X. S. Wang, P. Yan, Y. H. Shen, G. E. W. Bauer, and X. R. Wang, Domain Wall Propagation through Spin Wave Emission, Phys. Rev. Lett. **109**, 167209 (2012).

[12] W. Wang, M. Albert, M. Beg, M.-A. Bisotti, D. Chernyshenko, D. Cortés-Ortuño, I. Hawke, and H. Fangohr, Magnon-Driven Domain-Wall Motion with the Dzyaloshinskii-Moriya Interaction, Phys. Rev. Lett. **114**, 087203 (2015).

[13] A. A. Kovalev and Y. Tserkovnyak, Thermomagnonic spin transfer and Peltier effects in insulating magnets, Europhys. Lett. **97**, 67002 (2012).

[14] W. Jiang, P. Upadhyaya, Y. Fan, J. Zhao, M. Wang, L.-T. Chang, M. Lang, K. L. Wong, M. Lewis, Y.-T. Lin, J. Tang, S. Cherepov, X. Zhou, Y. Tserkovnyak, R. N. Schwartz, and K. L. Wang, Direct Imaging of Thermally Driven Domain Wall Motion in Magnetic Insulators, Phys. Rev. Lett. **110**, 177202 (2013).

[15] X. S. Wang and X. R. Wang, Thermodynamic theory for thermal-gradient-driven domain-wall motion, Phys. Rev. B **90**, 014414 (2014).

[16] F. Schlickeiser, U. Ritzmann, D. Hinzke, and U. Nowak, Role of Entropy in Domain Wall Motion in Thermal Gradients, Phys. Rev. Lett. **113**, 097201 (2014).

[17] H. Y. Yuan, Z. Yuan, K. Xia, and X. R. Wang, Influence of nonlocal damping on the field-driven domain wall motion, Phys. Rev. B **94**, 064415 (2016).

[18] D. A. Allwood, G. Xiong, C. C. Faulkner, D. Atkinson, D. Petit, and R. P. Cowburn, Magnetic domain-wall logic, Science **309**, 1688 (2005).

[19] S. S. P. Parkin, M. Hayashi, and L. Thomas, Magnetic domain-wall racetrack memory, Science **320**, 190 (2008).

[20] G. Beach, Beyond the speed limit, Nat. Mater. **9**, 959 (2010).

[21] O. Gomonay, T. Jungwirth, and J. Sinova, High Antiferromagnetic Domain Wall Velocity Induced by Néel Spin-Orbit Torques, Phys. Rev. Lett. **117**, 017202 (2016).

[22] T. Shiino, S. H. Oh, P. M. Haney, S.-W. Lee, G. Go, B.-G. Park, and K.-J. Lee, Antiferromagnetic Domain Wall Motion Driven by Spin-Orbit Torques, Phys. Rev. Lett. **117**, 087203 (2016).

[23] F. D. M. Haldane, Nonlinear Field Theory of Large-Spin Heisenberg Antiferromagnets: Semiclassically Quantized Solitons of the One-Dimensional Easy-Axis Néel State, Phys. Rev. Lett. **50**, 1153 (1983).

[24] H. Y. Yuan, W. Wang, M.-H. Yung, and X. R. Wang, Classification of magnetic forces acting on an antiferromagnetic domain wall, Phys. Rev. B **97**, 214434 (2018).

[25] S. K. Kim, Y. Tserkovnyak, and O. Tchernyshyov, Propulsion of a domain wall in an antiferromagnet by magnons, Phys. Rev. B **90**, 104406 (2014); Erratum: Propulsion of a domain wall in an antiferromagnet by magnons [Phys. Rev. B **90**, 104406 (2014)], **91**, 099904(E) (2015).

[26] H. R. Hilzinger and H. Kronmüller, Spin configuration and intrinsic coercive field of narrow domain walls in Co_5R-compounds, Phys. Status Solidi **54**, 593 (1972).

[27] K. S. Novoselov, A. K. Geim, S. V. Dubonos, E. W. Hill, and I. V. Grigorieva, Subatomic movements of a domain wall in the Peierls potential, Nature (London) **426**, 812 (2003).

[28] P. Yan and G. E. W. Bauer, Magnonic Domain Wall Heat Conductance in Ferromagnetic Wires, Phys. Rev. Lett. **109**, 087202 (2012).

[29] M. Bode, E. Y. Vedmedenko, K. von Bergmann, A. Kubetzka, P. Ferriani, S. Heinze, and R. Wiesendanger, Atomic spin structure of antiferromagnetic domain walls, Nat. Mater. **5**, 477 (2006).

[30] J. Železný, H. Gao, K. Výborný, J. Zemen, J. Mašek, A. Manchon, J. Wunderlich, J. Sinova, and T. Jungwirth, Relativistic Néel-Order Fields Induced by Electrical Current in Antiferromagnets, Phys. Rev. Lett. **113**, 157201 (2014).

[31] A. Vansteenkiste, J. Leliaert, M. Dvornik, M. Helsen, F. Garcia-Sanchez, and B. Van Waeyenberge, The design and verification of MUMAX3, AIP Adv. **4**, 107133 (2014).

[32] E. G. Tveten, T. Müller, J. Linder, and A. Brataas, Intrinsic magnetization of antiferromagnetic textures, Phys. Rev. B **93**, 104408 (2016).

[33] N. Papanicolaou, Antiferromagnetic domain walls, Phys. Rev. B **51**, 15062 (1995).

[34] H. Y. Yuan, M.-H. Yung, and X. R. Wang, Emergence of antiferromagnetic quantum domain walls, Phys. Rev. B **98**, 060407(R) (2018).

[35] Here we first extract the DW positions by fitting the n_z vs z curve using the Walker profile and then derive the DW velocity by linearly fitting the DW positions versus simulation time in the steady regime.

[36] M. Yan, C. Andreas, A. Kákay, F. Garcia-Sánchez, and R. Hertel, Fast domain wall dynamics in magnetic nanotubes: Suppression of Walker breakdown and Cherenkov-like spin wave emission, Appl. Phys. Lett. **99**, 122505 (2011).

[37] U. Atxitia, P. Nieves, and O. Chubykalo-Fesenko, Landau-Lifshitz-Bloch equation for ferrimagnetic materials, Phys. Rev. B **86**, 104414 (2012).

[38] E. C. Stoner and E. P. Wohlfarth, A mechanism of magnetic hysteresis in heterogeneous alloys, Philos. Trans. R. Soc. London, Ser. A **240**, 599 (1948).

[39] T. Devolder, P. Crozat, J.-V. Kim, C. Chappert, K. Ito, J. A. Katine, and M. J. Carey, Magnetization switching by spin torque using subnanosecond current pulses assisted by hard axis magnetic fields, Appl. Phys. Lett. **88**, 152502 (2006).

[40] M. Sato, T. Higuchi, N. Kanda, K. Konishi, K. Yoshioka, T. Suzuki, K. Misawa, and M. Kuwata-Gonokami, Terahertz polarization pulse shaping with arbitrary field control, Nat. Photonics **7**, 724 (2013).

[41] M. Yan, A. Kákay, S. Gliga, and R. Hertel, Beating the Walker Limit with Massless Domain Walls in Cylindrical Nanowires, Phys. Rev. Lett. **104**, 057201 (2010).

[42] Here there is a little difference between the minimum phase velocity of spin waves ($v_{\mathrm{p,min}} = 31\,\mathrm{km/s}$) and the conventional definition of magnon velocity ($c = 28.2\,\mathrm{km/s}$). It comes from the weak anisotropy, which is omitted in defining c [23].

[43] H. Y. Yuan, Q. Liu, K. Xia, Z. Yuan, and X. R. Wang, Proper dissipative torques in antiferromagnetic dynamics, arXiv:1801.00217.

[44] A. Kamra, R. Troncoso, W. Belzig, and A. Brataas, Gilbert damping phenomenology for two-sublattice magnets, Phys. Rev. B **98**, 184402 (2018).

[45] Q. Liu, H. Y. Yuan, K. Xia, and Z. Yuan, Mode-dependent damping in metallic antiferromagnets due to intersublattice spin pumping, Phys. Rev. Mater. **1**, 061401(R) (2017).

[46] F. Mahfouzi and N. Kioussis, Damping and antidamping phenomena in metallic antiferromagnets: An *ab initio* study, Phys. Rev. B **98**, 220410(R) (2018).

[47] C. A. Akosa, I. M. Miron, G. Gaudin, and A. Manchon, Phenomenology of chiral damping in noncentrosymmetric magnets, Phys. Rev. B **93**, 214429 (2016).

[48] E. Jué, C. K. Safeer, M. Drouard, A. Lopez, P. Balint, L. Buda-Prejbeanu, O. Boulle, S. Auffret, A. Schuhl, A. Manchon, I. M. Miron, and G. Gaudin, Chiral damping of magnetic domain walls, Nat. Mater. **15**, 272 (2016).

[49] C. A. Akosa, A. Takeuchi, Z. Yuan, and G. Tatara, Theory of chiral effects in magnetic textures with spin-orbit coupling, Phys. Rev. B **98**, 184424 (2018).

[50] K.-W. Kim, H.-W. Lee, K.-J. Lee, K. Everschor-Sitte, O. Gomonay, and J. Sinova, Roles of chiral renormalization on magnetization dynamics in chiral magnets, Phys. Rev. B **97**, 100402(R) (2018).

[51] A. A. Sapozhnik, C. Luo, H. Ryll, F. Radu, M. Jourdan, H. Zabel, and H.-J. Elmers, Experimental determination of exchange constants in antiferromagnetic Mn_2Au, Phys. Rev. B **97**, 184416 (2018).

[52] A. B. Shick, S. Khmelevskyi, O. N. Mryasov, J. Wunderlich, and T. Jungwirth, Spin-orbit coupling induced anisotropy effects in bimetallic antiferromagnets: A route towards antiferromagnetic spintronics, Phys. Rev. B **81**, 212409 (2010).